

Interplay between evolutionary and epidemic time scales challenges the outcome of control policies

Santiago Lamata-Otín ^{1,2} Alex Arenas ^{3,4,5,6} Jesús Gómez-Gardeñes ^{1,2,7} and David Soriano-Paños ^{3,2}

¹*Department of Condensed Matter Physics, University of Zaragoza, 50009 Zaragoza (Spain).*

²*GOTHAM lab, Institute for Biocomputation and Physics of Complex Systems (BIFI), University of Zaragoza, 50018 Zaragoza (Spain).*

³*Departament d'Enginyeria Informàtica i Matemàtiques, Universitat Rovira i Virgili, 43007 Tarragona, Spain*

⁴*Pacific Northwest National Laboratory, 902 Battelle Boulevard, Richland, Washington 99354, USA*

⁵*Complexity Science Hub Vienna, Metternichgasse 8, 1030 Vienna, Austria*

⁶*ComSCIAM, Universitat Rovira i Virgili, 43007 Tarragona, Spain*

⁷*Center for Computational Social Science, University of Kobe, 657-8501 Kobe (Japan).*

(Dated: March 20, 2026)

The SIR model is the cornerstone model for mathematical epidemiology, explaining key epidemic features such as the second-order transition between disease-free and epidemic states, the initial exponential growth of outbreaks or the short-term benefits of control measures. Nonetheless, the classical SIR model assumes that pathogen traits remain fixed, thus neglecting viral evolution. Here we propose a minimal extension of the SIR model, allowing infectiousness to evolve. We show that such evolution can cause superexponential early growth of outbreaks, create abrupt epidemic transitions, and undermine the effectiveness of control policies, as lifting interventions too early can lead to worse epidemic scenarios than no action. We derive analytical expressions for the critical mutation rate and intervention time governing this behavior, and identify a strong asymmetry between control strategies: while shortening the infectious period hinders transmission without suppressing viral evolution, lowering transmission both reduces cases and slows down viral evolution.

Introduction.— The dynamics of infectious diseases emerge from the interplay between pathogen traits and host populations [1, 2]. Classical epidemic models, such as the susceptible–infected–recovered (SIR) framework [3, 4], have been instrumental in understanding outbreak dynamics and in guiding the design of control strategies during recent pandemics [5–8]. Recent theoretical studies [9–13], and particularly the work of Morris et al. [14], have further analyzed how simple, fixed-strength interventions can be robust and near-optimal control strategies.

A key underlying assumption in these approaches is that pathogen traits remain effectively constant over the course of an outbreak. Yet, many pathogens evolve on timescales comparable to epidemic spreading, so that mutation can directly affect epidemic dynamics [15–19]. The impact of control policies on viral evolution has been mostly addressed in two-strain settings, characterizing analytically how interventions alter the emergence, survival and immune escape probabilities of mutants both within hosts [20–23] and at the population level [24–26]. Beyond the two-strain settings, phylodynamic approaches have proven substantial alterations in the evolutionary trajectories of Ebola and Influenza A viruses following non-pharmaceutical interventions applied to contain Ebola [27] or COVID-19 outbreaks respectively [28, 29].

The theoretical study of how viral evolution shapes epidemic trajectories and the effectiveness of control strategies in multi-strain settings has been much less explored

in the literature [30, 31]. In this Letter, we address these questions by introducing a minimal extension of the SIR model in which infectivity is an evolving pathogen trait. This framework allows us to couple epidemiological dynamics with evolutionary processes while retaining analytical tractability. We show that including evolution in the SIR model challenges the expected behavior of this model, inducing superexponential early-time dynamics or abrupt epidemic transitions and reverting the short-term benefits of epidemic control policies. We also show how the compatibility of evolutionary and epidemic time scales leads to strongly asymmetric outcomes of interventions shaping within-host or inter-host dynamics. Our results therefore show that epidemic control and pathogen evolution are intrinsically coupled and should therefore be studied jointly for rapidly evolving viruses.

Modeling epidemics with infectivity evolution.— We consider a minimal extension of the SIR model in which individuals are either susceptible (S), infected (I), or recovered (R), and where infectivity is an evolving trait (see Fig. 1a). For contagions, we assume that infected individuals make k contacts per time step, transmitting their associated strain to a susceptible contact with a probability λ , hereafter referred to as infectivity of that strain. We assume a competitive exclusion regime, therefore neglecting coinfections by multiple strains. Following [30–33], infectivity evolves in a one-dimensional trait space via symmetric mutations of size $\pm\Delta\lambda$ occurring at rate D . Finally, infected individuals recover at a rate μ , entering into the R compartment. The epidemic state of our

system is characterized by the probability density of infected individuals across the traits space $\rho_I(\lambda, t)$ and the global fraction of recovered $r(t)$ individuals. Taking into account the rules described above, the time evolution of these quantities read:

$$\frac{\partial \rho_I(\lambda, t)}{\partial t} = k \lambda \rho_I(\lambda, t) s(t) - \mu \rho_I(\lambda, t) + \frac{\mathcal{D}}{2} \frac{\partial^2 \rho_I(\lambda, t)}{\partial \lambda^2}, \quad (1)$$

$$\frac{dr(t)}{dt} = \mu i(t), \quad (2)$$

where $i(t) = \int d\lambda \rho_I(\lambda, t)$ and $s(t) = 1 - i(t) - r(t)$ are the disease prevalence and the fraction of susceptible individuals at time t respectively. For mathematical convenience, we have used an effective diffusion rate $\mathcal{D} = D(\Delta\lambda)^2$, which remains invariant under rescalings of D and $\Delta\lambda$ that keep $D(\Delta\lambda)^2$ constant (see Supplementary Note 1).

Eq. (1) is a reaction–diffusion equation in trait space, structurally equivalent to replicator–mutator dynamics under time-dependent selection coefficients (see Supplementary Note 1). In particular, the first term selects for strains with larger λ through transmission, mediated by the depletion of the pool of susceptible individuals $s(t)$ throughout the dynamics. Conversely, the last term shows how mutation dynamics is translated into a diffusion of infected individuals in the trait space.

Effect of infectivity evolution on epidemic trajectories.— To characterize the epidemic trajectories, we monitor the time evolution of both the epidemic prevalence $i(t)$ and the associated basic reproduction number defined as:

$$\mathcal{R}_0(t) = \frac{k \bar{\lambda}(t)}{\mu}, \quad (3)$$

with the average infectivity

$$\bar{\lambda}(t) = \frac{\int d\lambda \lambda \rho_I(\lambda, t)}{i(t)}. \quad (4)$$

Unless otherwise stated, both quantities are obtained from the numerical integration of Eqs. (1)–(2), assuming an initial condition where a single strain with basic reproduction number $R_0 = 2$ affects a tiny fraction $i_0 = 10^{-3}$ of the population, with $\mu = 1/7$ days $^{-1}$ and $k = 10$ contacts per day. For evolution, we assume a discrete representation of the trait space with $\Delta\lambda = 10^{-3}$ (see Supplementary Note 1).

Infectivity evolution qualitatively reshapes epidemic trajectories, inducing a super-exponential growth, advancing the epidemic peak and increasing its magnitude (Fig. 1b). Moreover, Fig. 1c shows that infectivity evolution presents an initial superlinear growth followed by a bending which is slowed down at later stages. Both results can be understood analytically from the dynamics

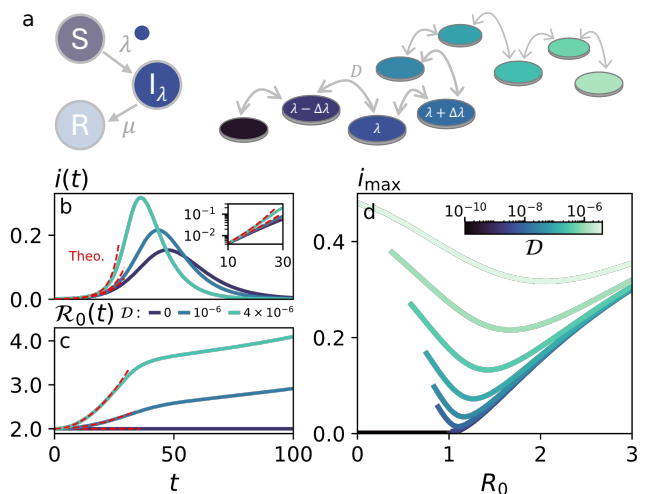


FIG. 1. Effect of infectivity evolution on epidemic trajectories. **a** Schematic illustration of the epidemic model with evolving infectivity. **b–c** Temporal evolution of the epidemic prevalence $i(t)$ (**b**) and basic reproduction number $\mathcal{R}_0(t)$ (**c**). **d** Epidemic peak i_{\max} as a function of the initial basic reproduction number R_0 for different values of \mathcal{D} , revealing an abrupt epidemic diagram induced by infectivity evolution. In panels **b** and **c**, dashed lines show the theoretical predictions from Eqs. (6)–(7), and we set $R_0 = 2$. In panels **b**, **c** and **d**, we set $i_0 = 10^{-3}$, $\mu = 1/7$, $k = 10$ and $\Delta\lambda = 10^{-3}$, and stop simulations if $i(t) < 10^{-4}$.

of the average infectivity. In the Supplementary Note 2, we show that differentiating Eq. (4) leads to

$$\frac{d\bar{\lambda}}{dt} = k s(t) \text{Var}(\lambda), \quad (5)$$

where $\text{Var}(\lambda)$ is the variance of λ values considering the prevalence distribution across traits $\rho_I(\lambda, t)$. The diffusive contribution yields $\text{Var}(\lambda) \simeq \mathcal{D}t$. For early-time dynamics, one can assume that $s(t) \simeq 1$. Combining both assumptions, we can integrate Eq. (4), yielding:

$$\bar{\lambda}(t)|_{t \rightarrow 0} = \lambda_0 + \frac{1}{2} k \mathcal{D} t^2, \quad (6)$$

which directly translates into a super-exponential growth of the prevalence,

$$i(t)|_{t \rightarrow 0} = i_0 \exp \left[\mu (R_0 - 1) t + \frac{k^2 \mathcal{D}}{6} t^3 \right]. \quad (7)$$

Note that infectivity evolution introduces an additional cubic term [30] in the growth exponent compared to the standard SIR model. Equations (6)–(7) accurately capture the early-time dynamics in Fig. 1b–c. As the epidemic progresses, the susceptible depletion slows down the growth of $\bar{\lambda}(t)$, producing the bending observed in Fig. 1c (see Appendix A for further details).

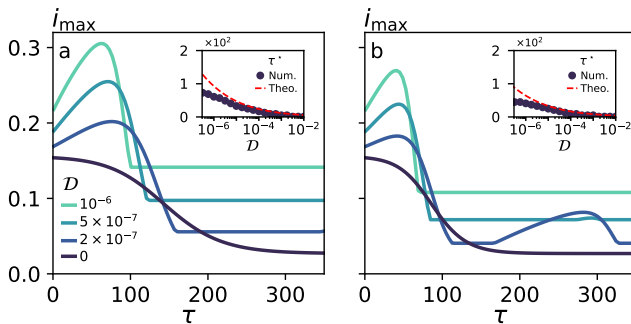


FIG. 2. **Effect of infectivity evolution on epidemic control.** **a** Epidemic peak i_{\max} under k - or λ -control as a function of the intervention time τ for different values of the effective diffusion rate \mathcal{D} . **b** Same as in **a** for μ -control. In both panels, inset represents the theoretical (red dashed line) prediction obtained with Eq. (11) and the numerical (blue dots) values for the peak of the critical intervention time yielding the highest i_{\max} value. In both panels we set $i_0 = 10^{-3}$, $R_0 = 2$, $\mu = 1/7$, $k = 10$ and $\varepsilon = 0.6$.

Effect of infectivity evolution on epidemic control.— The epidemic peak i_{\max} is a pivotal quantity for mathematical epidemiology, as it indicates the highest pressure on health systems during epidemic outbreaks. Figure 1d shows how the epidemic transition of the SIR model is strongly altered by evolution. While in the absence of evolution, i.e. $D = 0$, epidemic outbreaks occur through a second-order transition at $R_0 = 1$, increasing D gives rise to abrupt epidemic transitions occurring for lower R_0 values. This occurs because infectivity evolution enhances transmissibility during the outbreak, effectively pushing the dynamics into the supercritical region of the classical SIR phase diagram even when starting from marginally transmissible strains [30]. Moreover, the non-monotonic dependence of i_{\max} shows that evolutionary effects are amplified when outbreaks originate from less transmissible strains, as slower epidemic growth produces more transmission chains, thus fueling the evolution of viral infectivity.

The latter result represents a cautionary tale for the short-term benefits of control policies, as lowering the basic reproduction number can lead to a worse epidemic scenario. We now tackle this issue by addressing the impact of control policies on the epidemic curves of our model. Our interventions are characterized by two parameters [14]: the duration of the intervention τ and its strength ε . Namely, our intervention rescales the reproduction number, i.e. $\mathcal{R}_0(t) \rightarrow \varepsilon \mathcal{R}_0(t)$, with $\varepsilon \in (0, 1)$, over the intervention time τ . Eq. (3) shows that such goal can be achieved through three different strategies: (i) λ -control (reducing transmissibility as $\lambda \rightarrow \varepsilon \lambda$), (ii) k -control (reducing contacts as $k \rightarrow \varepsilon k$) and (iii) μ -control (shortening the infectious period via $\mu \rightarrow \mu/\varepsilon$). While the first two strategies are related to

inter-host transmission events, the last intervention aims at accelerating viral clearance within hosts. Unless otherwise stated, we set $\varepsilon = 0.6$ and treat k -control and λ -control jointly, which are equivalent within the model (see Supplementary Note 4).

In the absence of infectivity evolution, all policies monotonically reduce the epidemic peak as the intervention duration τ increases (see Fig. 2a for k - or λ -control and Fig. 2b for μ -control), implying that longer interventions are always beneficial. When evolution is considered, however, i_{\max} becomes a non-monotonic function of τ , initially increasing and then decreasing after reaching a maximum. Consequently, lifting a control policy too early may result in a larger epidemic peak than in the absence of intervention ($\tau = 0$).

This result can be captured analytically. As derived in Supplementary Note 4, the early-time evolution of the average infectivity under intervention is

$$\bar{\lambda}(t, \varepsilon)|_{t \rightarrow 0} = \lambda_0 + \frac{1}{2} \alpha k \mathcal{D} t^2, \quad (8)$$

where $\alpha = \varepsilon$ for k, λ -control, and $\alpha = 1$ for μ -control. As a consequence, the prevalence dynamics follows

$$i(t, \varepsilon)|_{t \rightarrow 0} = i_0 \exp \left[\frac{\mu \alpha}{\varepsilon} (\varepsilon R_0 - 1) t + \frac{\alpha^2 k^2}{6} \mathcal{D} t^3 \right]. \quad (9)$$

We can estimate the peak observed after lifting the intervention at $t = \tau$, hereafter denoted by $i_{\max}(\tau)$, by introducing $i(\tau)$ and $\lambda(\tau)$ in the usual expression of the epidemic peak of the SIR model (see Appendix B and Supplementary Note 4 for details). Differentiating i_{\max} with respect to τ yields:

$$\frac{di_{\max}}{d\tau} = -\mu i(\tau) \alpha \frac{(1 - \varepsilon)}{\varepsilon} + \frac{\alpha k^2}{\mu} \mathcal{D} \tau \frac{\ln(\mathcal{R}_0(\tau) s(\tau))}{\mathcal{R}_0(\tau)^2}. \quad (10)$$

This expression makes explicit the competition between epidemiological suppression (first term) and evolutionary amplification (second term) for short intervention durations. In particular, given an intervention duration τ , the sign of the derivative changes at a critical diffusion strength \mathcal{D}_c (detailed explicitly in the Appendix C and in Supplementary Note 4), what pinpoints that interventions improve (worsen) the epidemic scenario for viruses with $\mathcal{D} < \mathcal{D}_c$ ($\mathcal{D} > \mathcal{D}_c$).

Considering $\mathcal{D} > \mathcal{D}_c$, we can also estimate the duration of the intervention τ^* producing the worst epidemic scenario, i.e. the maximum value of the epidemic peak i_{\max} . Imposing $\left. \frac{di_{\max}}{d\tau} \right|_{\tau=\tau^*} = 0$ yields (see Supplementary Note 4 for details):

$$\tau^* \simeq \left[-\frac{1}{3B\mathcal{D}} W_{-1} \left(-\frac{3B\mu^3(1-\varepsilon)^3 i_0^3}{\varepsilon^3 C^3 \mathcal{D}^2} \right) \right]^{1/3}, \quad (11)$$

with $B = \alpha^2 k^2 / 6$ and $C = k^2 \ln R_0 / (\mu R_0^2)$. W_{-1} denotes one of the branches of the Lambert function W , which fulfills $W(z)e^{W(z)} = z$. The resulting analytical predictions are in quantitative agreement with numerical simulations (see insets in Fig. 2), particularly for large values of \mathcal{D} , where the characteristic dynamical timescale is reduced. For completeness, in the Supplementary Note 5 we assess the influence of the basic reproduction number R_0 , policy strength ε , and the intervention activation threshold, showing that the nonmonotonic behavior is robust.

Asymmetric effect of control policies shaping inter-host or within-host dynamics.— Comparing Figs. 2a-b, we observe a difference between k, λ -control, and μ -control. In the absence of infectivity evolution, *i.e.*, the usual SIR model, shortening the infectious period yields a smaller post-lifting peak than reducing transmissibility. We observe that infectivity evolution amplifies this effect for short interventions whereas it might revert it for longer interventions, as highlighted by the secondary peak appearing for $\mathcal{D} = 2 \times 10^{-7}$ in Fig. 2b.

The impact of the difference between interventions is made explicit in Fig. 3a, which shows $\Delta i_{\max} = i_{\max}^{(k, \lambda)} - i_{\max}^{(\mu)}$. Considering a constant \mathcal{D} value, *e.g.* $\mathcal{D} = 10^{-6}$, we first observe that increasing τ yields a transition from a similar outcome of both interventions ($\Delta i_{\max} \simeq 0$) to a substantially larger epidemic peak after k, λ -control compared to the one observed after μ -control. Note that this transition also appears in absence of evolution, *i.e.* very low \mathcal{D} values, but evolution exacerbates it and anticipates its onset.

To gain insights into this transition, we represent the epidemic trajectories $i(t)$ along with the evolution of the basic reproduction number $\mathcal{R}_0(t)$ and the pool of susceptible individuals $s(t)$ for $\tau = 30$ days (Fig. 3b) and $\tau = 75$ days (Fig. 3c). Comparing the curves of susceptible individuals, we can observe how the acceleration of the epidemic time scales triggered by μ -control leads to a faster depletion of the pool of susceptible individuals. While this faster depletion is not substantial for very short interventions (Fig. 3b), it becomes evident once the peak of the μ -control epidemic curves has been reached (Fig. 3b). In that case, the exhausted pool of susceptible individuals prevents the emergence of another major outbreak, as observed in the case of the k, λ -control. Using this intuition, the region of strong asymmetry should be delimited by those intervention times yielding the highest epidemic peaks for both interventions, *i.e.* τ_{μ}^* and $\tau_{k, \lambda}^*$. Thus, we can compute them with Eq. (11), using the α value of each policy. The red dashed lines in Fig. 3a show a fair agreement between our theoretical bounds for this region and the results from numerical simulations.

Fig. 3a also illustrates that longer interventions and moderate evolutionary rates revert the asymmetric out-

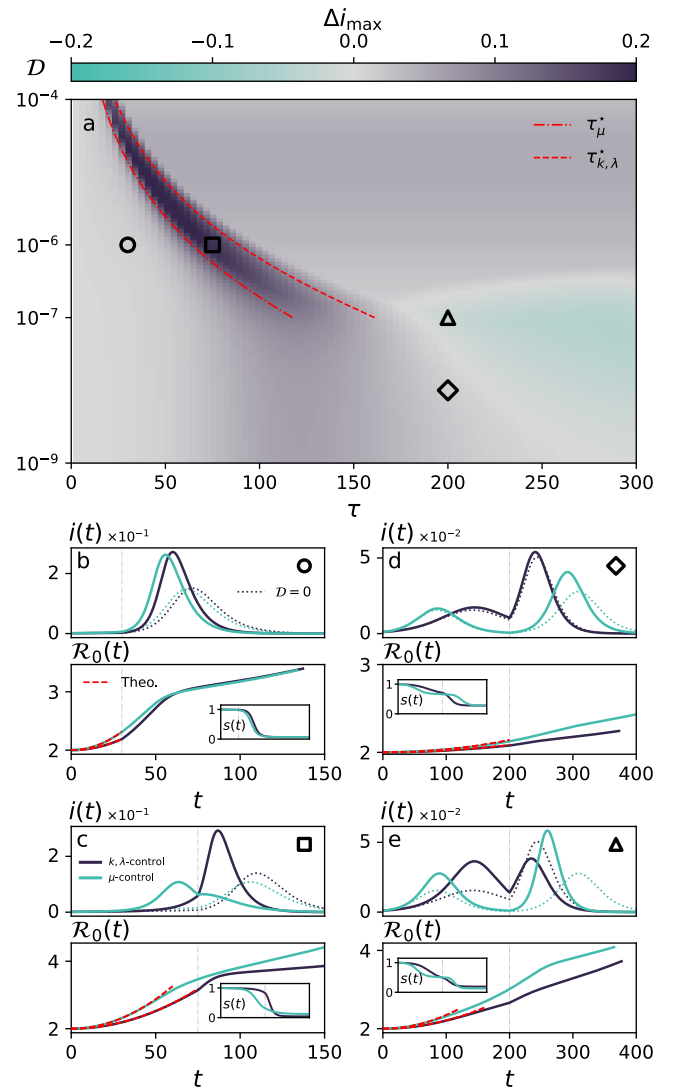


FIG. 3. Asymmetric effect of control policies. **a** Difference in epidemic peak Δi_{\max} between the k, λ -control and μ -control as a function of τ and \mathcal{D} . Dashed curves indicate the theoretical predictions for the critical intervention durations τ^* associated with each strategy. **b-e** Temporal evolution of the epidemic prevalence $i(t)$ (top row) and the corresponding time-varying basic reproduction number $\mathcal{R}_0(t)$ (bottom row) for (b) $\tau = 30$ and $\mathcal{D} = 10^{-6}$, (c) $\tau = 75$ and $\mathcal{D} = 10^{-6}$, (d) $\tau = 200$ and $\mathcal{D} = 10^{-8}$ and (e) $\tau = 200$ and $\mathcal{D} = 10^{-7}$. Panels **b-e** include the theoretical prediction for the early-time dynamics (red dashed line) and, in the inset, the evolution of the susceptible population $s(t)$. Moreover, we stop simulations if $i(t) < 10^{-4}$. In all panels, we set $i_0 = 10^{-3}$, $R_0 = 2$, $\mu = 1/7$, $k = 10$ and $\varepsilon = 0.6$. Colors distinguish control strategies, as indicated in panel **c**, and vertical lines indicate lifting times. Symbols in panel **a** correspond to the parameter choices shown in panels **b-e**.

come of control policies, producing a higher peak for the μ -control strategy, *i.e.* $\Delta i_{\max} \leq 0$. To understand this phenomenon, we consider $\tau = 200$ and represent the

epidemic and evolutionary curves assuming $\mathcal{D} = 10^{-8}$ (Fig. 3d) and $\mathcal{D} = 10^{-7}$ (Fig. 3e). In both cases, $s(t)$ does not allow us to explain the unequal outcome, as the pool of susceptible individuals is only partially depleted and of similar size for each strategy. We should instead focus on how the different control policies shape the evolution of the virus. While μ -control yields the same early-time evolution of \mathcal{R}_0 as in the uncontrolled case, k, λ -control slows down viral evolution. Eq. (8) captures this difference, encoded in the parameter α , with a fair agreement between the theoretical lines and the numerical results at early stages of the outbreak.

Therefore, for intermediate evolutionary speeds, i.e. $\mathcal{D} \sim 10^{-7}$, the pool of susceptible agents is large and of similar size across strategies at $t = \tau$. However, viruses under μ -control have much higher infectiousness than those under k, λ -control, thus explaining the higher epidemic peak in the secondary outbreak [34]. Note that this behavior does not appear for faster evolutionary rates as they induce a much greater depletion of the susceptible population, not observing any secondary peak.

Conclusions.— We have shown that allowing pathogen infectivity to evolve reshapes in a fundamental way both epidemic dynamics and the effectiveness of control strategies. The interplay between contagion (selection) and mutation (diffusion) induces superexponential early-time prevalence growth (consistent with previous findings by Zhang et al. [30]), and an abrupt epidemic phase diagram, positioning trait evolution as an additional pathway towards explosive transitions in contagion dynamics [35–37].

When control measures are incorporated, these evolutionary effects lead to qualitatively different and counterintuitive outcomes. In particular, the epidemic peak depends nonmonotonically on intervention duration, implying that prematurely lifted interventions may worsen epidemic outcomes relative to doing nothing. Furthermore, we identified an asymmetry between control strategies: interventions acting on transmission parameters and those shortening the infectious period are no longer equivalent in the presence of infectivity evolution. Shortening the infectious period, e.g. by administering drugs, accelerates epidemic timescales without slowing infectivity evolution, whereas acting on inter-host transmission slows both prevalence and infectivity growth. As a result, the relative effectiveness of control strategies may be reversed: policies that appear optimal in non-evolving settings can become counterproductive once evolutionary effects are taken into account, particularly when interventions are lifted after the first epidemic peak.

Overall, we have introduced a minimal model revealing a natural multiscale coupling between mutation dynamics within hosts and epidemic control at the population level, which determines the selection of newly emerging variants and, consequently, viral evo-

lution. Despite the simplicity of the model here introduced, our findings are quite general and expected to appear in more biologically-grounded models including complementary evolutionary pathways such as antigenic drift [31, 38–40], exhaustive descriptions of within-host dynamics [41, 42] or evolutionary trade-offs constraining viral evolution [43–45].

Acknowledgments— S.L.O and J.G.G. acknowledge financial support from the Departamento de Industria e Innovación del Gobierno de Aragón y Fondo Social Europeo (FENOL group grant E36-23R) and from Ministerio de Ciencia e Innovación (grant PID2023-147734NB-I00). S.L.O. acknowledges financial support from Gobierno de Aragón through a doctoral fellowship. A.A. and D.S.-P acknowledge Spanish Ministerio de Ciencia e Innovación (PID2024-158120NB-C21). AA acknowledges Generalitat de Catalunya (2021SGR-00633), Universitat Rovira i Virgili (2023PFR-URV-00633), the European Union’s Horizon Europe Programme under the CREX-DATA project (grant agreement no. 101092749), ICREA Academia, the James S. McDonnell Foundation (Grant N. 220020325), and the Joint Appointment Program at Pacific Northwest National Laboratory (PNNL). PNNL is a multi-program national laboratory operated for the U.S. Department of Energy (DOE) by Battelle Memorial Institute under Contract No. DE-AC05-76RL01830.

Code availability— The code is available at <https://github.com/santiagolaot/SIREvolution>.

-
- [1] M. J. Keeling and P. Rohani, *Modeling infectious diseases in humans and animals* (Princeton university press, 2008).
 - [2] R. Pastor-Satorras, C. Castellano, P. Van Mieghem, and A. Vespignani, Epidemic processes in complex networks, *Reviews of modern physics* **87**, 925 (2015).
 - [3] W. O. Kermack and A. G. McKendrick, A contribution to the mathematical theory of epidemics, *Proceedings of the royal society of london. Series A, Containing papers of a mathematical and physical character* **115**, 700 (1927).
 - [4] H. W. Hethcote, The mathematics of infectious diseases, *SIAM review* **42**, 599 (2000).
 - [5] S. Flaxman, S. Mishra, A. Gandy, H. J. T. Unwin, T. A. Mellan, H. Coupland, C. Whittaker, H. Zhu, T. Berah, J. W. Eaton, *et al.*, Estimating the effects of non-pharmaceutical interventions on covid-19 in europe, *Nature* **584**, 257 (2020).
 - [6] S. Hsiang, D. Allen, S. Annan-Phan, K. Bell, I. Boliger, T. Chong, H. Druckenmiller, L. Y. Huang, A. Hultgren, E. Krasovich, *et al.*, The effect of large-scale anti-contagion policies on the covid-19 pandemic, *Nature* **584**, 262 (2020).
 - [7] S. M. Kissler, C. Tedijanto, E. Goldstein, Y. H. Grad, and M. Lipsitch, Projecting the transmission dynamics of sars-cov-2 through the postpandemic period, *Science* **368**, 860 (2020).

- [8] A. Arenas, W. Cota, J. Gómez-Gardeñes, S. Gómez, C. Granell, J. T. Matamalas, D. Soriano-Paños, and B. Steinegger, Modeling the spatiotemporal epidemic spreading of covid-19 and the impact of mobility and social distancing interventions, *Physical Review X* **10**, 041055 (2020).
- [9] F. Di Lauro, I. Z. Kiss, and J. C. Miller, Optimal timing of one-shot interventions for epidemic control, *PLOS Computational Biology* **17**, e1008763 (2021).
- [10] P.-A. Bliman, M. Duprez, Y. Privat, and N. Vauchelet, Optimal immunity control and final size minimization by social distancing for the sir epidemic model, *Journal of Optimization Theory and Applications* **189**, 408 (2021).
- [11] D. I. Ketcheson, Optimal control of an sir epidemic through finite-time non-pharmaceutical intervention, *Journal of mathematical biology* **83**, 7 (2021).
- [12] T. A. Perkins and G. España, Optimal control of the covid-19 pandemic with non-pharmaceutical interventions, *Bulletin of mathematical biology* **82**, 118 (2020).
- [13] J. Hindes and I. B. Schwartz, Epidemic extinction and control in heterogeneous networks, *Physical review letters* **117**, 028302 (2016).
- [14] D. H. Morris, F. W. Rossine, J. B. Plotkin, and S. A. Levin, Optimal, near-optimal, and robust epidemic control, *Communications Physics* **4**, 78 (2021).
- [15] B. T. Grenfell, O. G. Pybus, J. R. Gog, J. L. Wood, J. M. Daly, J. A. Mumford, and E. C. Holmes, Unifying the epidemiological and evolutionary dynamics of pathogens, *science* **303**, 327 (2004).
- [16] R. M. Anderson and R. M. May, *Infectious diseases of humans: dynamics and control* (Oxford university press, 1991).
- [17] T. Day and S. Gandon, Applying population-genetic models in theoretical evolutionary epidemiology, *Ecology Letters* **10**, 876 (2007).
- [18] S. Lion and J. A. Metz, Beyond r_0 maximisation: on pathogen evolution and environmental dimensions, *Trends in ecology & evolution* **33**, 458 (2018).
- [19] L. S. Tsimring, H. Levine, and D. A. Kessler, Rna virus evolution via a fitness-space model, *Physical review letters* **76**, 4440 (1996).
- [20] Y. Iwasa, F. Michor, and M. A. Nowak, Evolutionary dynamics of escape from biomedical intervention, *Proceedings of the Royal Society of London. Series B: Biological Sciences* **270**, 2573 (2003).
- [21] Y. Iwasa, F. Michor, and M. A. Nowak, Evolutionary dynamics of invasion and escape, *Journal of Theoretical Biology* **226**, 205 (2004).
- [22] M. Hartfield and S. Alizon, Within-host stochastic emergence dynamics of immune-escape mutants, *PLoS computational biology* **11**, e1004149 (2015).
- [23] D. Van Egeren, A. Novokhodko, M. Stoddard, U. Tran, B. Zetter, M. S. Rogers, D. Joseph-McCarthy, and A. Chakravarty, Controlling long-term sars-cov-2 infections can slow viral evolution and reduce the risk of treatment failure, *Scientific reports* **11**, 22630 (2021).
- [24] M. Hartfield and S. Alizon, Epidemiological feedbacks affect evolutionary emergence of pathogens, *The American Naturalist* **183**, E105 (2014).
- [25] M. T. Meehan, R. C. Cope, and E. S. McBryde, On the probability of strain invasion in endemic settings: accounting for individual heterogeneity and control in multi-strain dynamics, *Journal of theoretical biology* **487**, 110109 (2020).
- [26] B. Ashby, C. A. Smith, and R. N. Thompson, Non-pharmaceutical interventions and the emergence of pathogen variants, *Evolution, Medicine, and Public Health* **11**, 80 (2023).
- [27] S. Dellicour, G. Baele, G. Dudas, N. R. Faria, O. G. Pybus, M. A. Suchard, A. Rambaut, and P. Lemey, Phylodynamic assessment of intervention strategies for the west african ebola virus outbreak, *Nature communications* **9**, 2222 (2018).
- [28] Z. Chen, J. L.-H. Tsui, B. Gutierrez, S. Busch Moreno, L. Du Plessis, X. Deng, J. Cai, S. Bajaj, M. A. Suchard, O. G. Pybus, *et al.*, Covid-19 pandemic interventions reshaped the global dispersal of seasonal influenza viruses, *Science* **386**, eadq3003 (2024).
- [29] Z. Chen, J. L.-H. Tsui, J. Cai, S. Su, C. Viboud, L. Du Plessis, P. Lemey, M. U. Kraemer, and H. Yu, Disruption of seasonal influenza circulation and evolution during the 2009 h1n1 and covid-19 pandemics in south-eastern asia, *Nature Communications* **16**, 475 (2025).
- [30] X. Zhang, Z. Ruan, M. Zheng, J. Zhou, S. Boccaletti, and B. Barzel, Epidemic spreading under mutually independent intra-and inter-host pathogen evolution, *Nature communications* **13**, 6218 (2022).
- [31] D. Soriano-Paños, Eco-evolutionary constraints for the endemicity of rapidly evolving viruses, *PRX Life* **3**, 043001 (2025).
- [32] I. M. Rouzine and G. Rozhnova, Antigenic evolution of viruses in host populations, *PLoS pathogens* **14**, e1007291 (2018).
- [33] V. Chardès, A. Mazzolini, T. Mora, and A. M. Walczak, Evolutionary stability of antigenically escaping viruses, *Proceedings of the National Academy of Sciences* **120**, e2307712120 (2023).
- [34] P. Castioni, S. Gómez, C. Granell, and A. Arenas, Rebound in epidemic control: How misaligned vaccination timing amplifies infection peaks, *npj Complexity* **1**, 20 (2024).
- [35] R. M. D'Souza, J. Gómez-Gardenes, J. Nagler, and A. Arenas, Explosive phenomena in complex networks, *Advances in Physics* **68**, 123 (2019).
- [36] S. Lamata-Otín, J. Gómez-Gardeñes, and D. Soriano-Paños, Pathways to discontinuous transitions in interacting contagion dynamics, *Journal of Physics: Complexity* **5**, 015015 (2024).
- [37] S. Lamata-Otín, A. Reyna-Lara, D. Soriano-Paños, V. Latora, and J. Gómez-Gardeñes, Collapse transition in epidemic spreading subject to detection with limited resources, *Physical Review E* **108**, 024305 (2023).
- [38] A. Sasaki, S. Lion, and M. Boots, Antigenic escape selects for the evolution of higher pathogen transmission and virulence, *Nature ecology & evolution* **6**, 51 (2022).
- [39] S. Lamata-Otín, O. C. Rotita-Ion, A. Arenas, D. Soriano-Paños, and J. Gómez-Gardeñes, Genotype networks drive oscillating endemicity and epidemic trajectories in viral evolution, *Communications Physics* (2025).
- [40] B. J. Williams, G. St-Onge, and L. Hébert-Dufresne, Localization, epidemic transitions, and unpredictability of multistrain epidemics with an underlying genotype network, *PLoS Computational Biology* **17**, e1008606 (2021).
- [41] N. Mideo, S. Alizon, and T. Day, Linking within-and between-host dynamics in the evolutionary epidemiology of infectious diseases, *Trends in ecology & evolution* **23**, 511 (2008).
- [42] F. Fabre, J. Montarry, J. Coville, R. Senoussi, V. Si-

mon, and B. Moury, Modelling the evolutionary dynamics of viruses within their hosts: a case study using high-throughput sequencing, *PLoS Pathogens* **8**, e1002654 (2012).

[43] S. Alizon, Transmission-recovery trade-offs to study parasite evolution, *The American Naturalist* **172**, E113 (2008).

[44] J. C. De Roode, A. J. Yates, and S. Altizer, Virulence-

transmission trade-offs and population divergence in virulence in a naturally occurring butterfly parasite, *Proceedings of the national academy of sciences* **105**, 7489 (2008).

[45] M. A. Acevedo, F. P. Dilleuth, A. J. Flick, M. J. Faldyn, and B. D. Elder, Virulence-driven trade-offs in disease transmission: A meta-analysis, *Evolution* **73**, 636 (2019).

End Matter

Appendix A: Sigmoid approximation for susceptible depletion— To analyze the slowdown in the growth of the average infectivity induced by susceptible depletion, we approximate the susceptible fraction by a sigmoid function centered at the epidemic peak, $s(t) \simeq s(\infty) + (1 - s(\infty))/(1 + e^{\sigma(t-t_p)})$. Substituting this expression into Eq. (5) and integrating yields an explicit approximation for the evolution of the average infectivity at intermediate times (see Supplementary Note 3). Retaining the dominant contribution for times around and beyond the peak time t_p , we obtain

$$\bar{\lambda}(t) \sim k\mathcal{D} \quad (\text{A1})$$

$$\times \left[s(\infty) \frac{t^2}{2} - (1 - s(\infty)) \left(\frac{t - t_p}{\sigma} e^{-\sigma(t-t_p)} \right) \right],$$

which explicitly displays a negative transient contribution that temporarily hinders the growth of infectivity (see Fig. 1c). As time increases, the exponential term vanishes and the dynamics smoothly crosses over to a quadratic growth controlled by the remaining susceptible fraction $s(\infty)$.

Appendix B: Hybrid approximation to derive the epidemic peak— To assess the impact of infectivity evolution on the effectiveness of control policies, we adopt a hybrid approximation in which the epidemic dynamics during the intervention window $t \in [0, \tau]$ follows the early-time controlled evolution of $i(t, \varepsilon)$ and $\bar{\lambda}(t, \varepsilon)$, while after lifting the intervention the outbreak evolves as an uncontrolled SIR process, with initial conditions given by the state at $t = \tau$ (see Supplementary Note 4 for details).

Under this approximation, and assuming that the epidemic peak occurs after lifting the intervention, the post-intervention peak can be approximated using the standard SIR result [37]

$$i_{\max}(\tau) \approx 1 - r(\tau) - \frac{1}{\mathcal{R}_0(\tau)} [1 + \ln(\mathcal{R}_0(\tau)s(\tau))], \quad (\text{A2})$$

where $\mathcal{R}_0(\tau) = k\bar{\lambda}(\tau)/\mu$ and $s(\tau) = 1 - i(\tau) - r(\tau)$. Note that this expression is a strong assumption as it neglects the impact of evolution on the epidemic peak; evolution just affects the initial conditions when lifting the intervention.

Differentiating Eq. (A2) with respect to τ and using the expressions for the controlled dynamics at the lifting

time [Eqs. (8)–(9)] yields the general identity reported in Eq. (10), which explicitly separates the direct epidemiological contribution from the evolutionary one.

Appendix C: Critical effective diffusion strength— To quantify when infectivity evolution reverses the monotonic dependence of the epidemic peak on the intervention duration, we analyze the condition $di_{\max}/d\tau = 0$, reported in Eq. (10) and derived in Appendix B. Setting $di_{\max}/d\tau = 0$ defines an implicit relation for the critical effective diffusion strength,

$$\mathcal{D}_c(\tau) = \frac{\mu^2(1 - \varepsilon) i(\tau) \mathcal{R}_0(\tau)^2}{\varepsilon k^2 \tau \ln(\mathcal{R}_0(\tau)s(\tau))}. \quad (\text{A3})$$

Assuming that the epidemic prevalence remains small at the lifting time, $i(\tau) \ll 1$, we approximate $s(\tau) \simeq 1$ and $\ln(\mathcal{R}_0(\tau)s(\tau)) \simeq \ln R_0$, and evaluate the logarithmic and prefactor terms at their zeroth-order values, $\mathcal{R}_0(\tau) \simeq R_0$, while retaining only the leading dependence on \mathcal{D} through the exponential contribution in $i(\tau)$. As detailed in Supplementary Note 5, under these approximations and using Eq. (9), Eq. (A3) reduces to a transcendental equation that admits a closed-form solution in terms of the Lambert W function,

$$\mathcal{D}_c(\tau) = -\frac{1}{P(\tau)} W_0[-P(\tau)Q(\tau)], \quad (\text{A4})$$

where $P(\tau) = \alpha^2 k^2 \tau^3 / 6$ and $Q(\tau) = (\mu^2(1 - \varepsilon) R_0^2) / (\varepsilon k^2 \tau \ln R_0) i_0 \exp[\mu\alpha(\varepsilon R_0 - 1)\tau/\varepsilon]$. In the expression above $\alpha = \varepsilon$ for k - or λ -control and $\alpha = 1$ for μ -control.

Equation (A4) exhibits a divergence $\mathcal{D}_c(\tau) \rightarrow \infty$ as $\tau \rightarrow 0$, reflecting the fact that the hybrid approximation accounts for infectivity evolution only during the controlled phase and therefore does not capture the $\tau \rightarrow 0$ limit. For finite intervention durations, however, it predicts a critical effective diffusion strength such that, for $\mathcal{D} > \mathcal{D}_c(\tau)$ the epidemic peak increases with the intervention duration, whereas for $\mathcal{D} < \mathcal{D}_c(\tau)$ it decreases.

SUPPLEMENTARY NOTE 1: COEVOLUTIONARY MODEL

Mapping to replicator–mutator dynamics

Integrating Eq. (1) in the main text over λ yields

$$\frac{di}{dt} = (ks(t)\bar{\lambda}(t) - \mu) i(t), \quad (\text{S.1})$$

where $i(t) = \int d\lambda \rho_I(\lambda, t)$ and $\bar{\lambda}(t) = (\int d\lambda \lambda \rho_I(\lambda, t)) / (\int d\lambda \rho_I(\lambda, t))$. We now introduce the normalized trait distribution $x(\lambda, t) = \frac{\rho_I(\lambda, t)}{i(t)}$, such that $\int d\lambda x(\lambda, t) = 1$. Taking the time derivative of $x(\lambda, t)$,

$$\frac{\partial x}{\partial t} = \frac{1}{i} \frac{\partial \rho_I}{\partial t} - \frac{\rho_I}{i^2} \frac{\partial i}{\partial t}, \quad (\text{S.2})$$

and substituting Eq. (1) together with Eq. (S.1), we obtain after rearranging terms

$$\frac{\partial x(\lambda, t)}{\partial t} = ks(t)(\lambda - \bar{\lambda}(t))x(\lambda, t) + \frac{\mathcal{D}}{2} \frac{\partial^2 x(\lambda, t)}{\partial \lambda^2}. \quad (\text{S.3})$$

Equation (S.3) has the structure of a continuous replicator–mutator equation: the selection term $ks(t)(\lambda - \bar{\lambda}(t))x$ represents fitness-dependent growth relative to the population mean, while the diffusion term $(\mathcal{D}/2)\partial_{\lambda\lambda}x$ models mutation in trait space. The effective fitness $f(\lambda, t) = k\lambda s(t)$ depends on the global susceptible fraction $s(t)$, which acts as a time-dependent mean field encoding resource depletion.

Discrete formulation

Starting from the continuum trait dynamics,

$$\frac{\partial \rho_I(\lambda, t)}{\partial t} = k \lambda \rho_I(\lambda, t) s(t) - \mu \rho_I(\lambda, t) + \frac{\mathcal{D}}{2} \frac{\partial^2 \rho_I(\lambda, t)}{\partial \lambda^2}, \quad (\text{S.4})$$

we discretize trait space as $\lambda_i = \lambda_0 + i \Delta\lambda$ and define $\rho_i^I(t) \equiv \rho_I(\lambda_i, t)$. Using the centered finite-difference approximation,

$$\left. \frac{\partial^2 \rho_I}{\partial \lambda^2} \right|_{\lambda=\lambda_i} \simeq \frac{\rho_{i-1}^I - 2\rho_i^I + \rho_{i+1}^I}{(\Delta\lambda)^2}, \quad (\text{S.5})$$

Eq. (S.4) becomes

$$\dot{\rho}_i^I = \lambda_i k \rho_i^I s - \mu \rho_i^I + \frac{\mathcal{D}}{2(\Delta\lambda)^2} (\rho_{i-1}^I - 2\rho_i^I + \rho_{i+1}^I). \quad (\text{S.6})$$

Introducing the discrete mutation operator $\Delta\rho_i^I \equiv \frac{\rho_{i-1}^I + \rho_{i+1}^I}{2} - \rho_i^I$, we can rewrite Eq. (S.6) as

$$\dot{\rho}_i^I = \lambda_i k \rho_i^I s - \mu \rho_i^I + D \Delta\rho_i^I, \quad D \equiv \frac{\mathcal{D}}{(\Delta\lambda)^2}. \quad (\text{S.7})$$

Therefore, changing the discretization $\Delta\lambda \rightarrow a \Delta\lambda$ can be exactly compensated by $D \rightarrow D/a^2$, leaving the continuum parameter $\mathcal{D} = D(\Delta\lambda)^2$ invariant.

SUPPLEMENTARY NOTE 2: EARLY-TIME DYNAMICS

In this Supplementary Note we derive the coupled evolution of the average infectivity and the epidemic prevalence, making explicit the respective roles of selection and mutation in shaping the early-time dynamics. We start considering the discrete version of the model introduced in Eq. (S.7), where the density of infected individuals carrying infectivity λ_i evolves as

$$\dot{\rho}_i^I = \lambda_i k \rho_i^I s - \mu \rho_i^I + D \Delta \rho_i^I, \quad \Delta \rho_i^I = \frac{\rho_{i-1}^I + \rho_{i+1}^I}{2} - \rho_i^I, \quad (\text{S.8})$$

with $s(t) = 1 - \sum_i \rho_i^I(t) - r(t)$. We recall that the total prevalence and the average infectivity are defined as

$$i(t) \equiv \sum_i \rho_i^I(t), \quad \bar{\lambda}(t) \equiv \frac{\sum_i \lambda_i \rho_i^I(t)}{\sum_i \rho_i^I(t)}. \quad (\text{S.9})$$

Evolution of the average infectivity

Let $A(t) \equiv \sum_i \lambda_i \rho_i^I(t)$ and $B(t) \equiv \sum_i \rho_i^I(t) = i(t)$, so that $\bar{\lambda} = A/B$. Differentiating the average infectivity yields

$$\dot{\bar{\lambda}} = \frac{\dot{A}}{B} - \bar{\lambda} \frac{\dot{B}}{B}. \quad (\text{S.10})$$

Using Eq. (S.8),

$$\dot{A} = ks \sum_i \lambda_i^2 \rho_i^I - \mu \sum_i \lambda_i \rho_i^I + D \sum_i \lambda_i \Delta \rho_i^I, \quad (\text{S.11})$$

$$\dot{B} = ks \sum_i \rho_i^I - \mu \sum_i \rho_i^I. \quad (\text{S.12})$$

Substituting Eqs. (S.11)–(S.12) into Eq. (S.10), the recovery terms cancel and we obtain

$$\dot{\bar{\lambda}}(t) = ks(t) \text{Var}(\lambda; t) + D \frac{\sum_i \lambda_i \Delta \rho_i^I(t)}{\sum_i \rho_i^I(t)}, \quad (\text{S.13})$$

where $\text{Var}(\lambda; t) \equiv \frac{\sum_i \lambda_i^2 \rho_i^I(t)}{\sum_i \rho_i^I(t)} - \bar{\lambda}(t)^2$ is the prevalence-weighted variance of infectivity. To lighten the notation, we will omit the time dependence in the variance in what follows.

Equation (S.13) separates two contributions. The first term is a *selection* term: transmission favors larger λ , so the mean infectivity increases proportionally to the width of the trait distribution, modulated by the susceptible fraction $s(t)$. The second term is a *mutation* term, representing the net drift of the first moment induced by diffusion in trait space. We note that the mutation term is a discrete divergence (the net difference of nearest-neighbor fluxes in trait space). Using $\lambda_{i+1} - \lambda_i = \Delta \lambda$, it can be rewritten as

$$\sum_i \lambda_i \Delta \rho_i^I = \frac{1}{2} \sum_i \lambda_i (\rho_{i+1}^I - 2\rho_i^I + \rho_{i-1}^I) = \frac{\Delta \lambda}{2} \left(\sum_i \rho_{i+1}^I - \sum_i \rho_{i-1}^I \right), \quad (\text{S.14})$$

which vanishes for symmetric trait domains with negligible density at the boundaries (or, equivalently, under no-flux boundary conditions). Therefore, at leading order,

$$\dot{\bar{\lambda}}(t) \simeq ks(t) \text{Var}(\lambda). \quad (\text{S.15})$$

Diffusive growth of trait variance

To close Eq. (S.15) we determine the time evolution of $\text{Var}(\lambda)$. Let $M_2(t) \equiv \sum_i \lambda_i^2 \rho_i^I(t)$, which corresponds to the second (non-central) moment of the infectivity distribution weighted by the infected density. Differentiating $\text{Var}(\lambda) = M_2/B - \bar{\lambda}^2$ gives

$$\frac{d}{dt} \text{Var}(\lambda) = \frac{\dot{M}_2}{B} - \frac{M_2}{B^2} \dot{B} - 2\bar{\lambda} \dot{\bar{\lambda}}. \quad (\text{S.16})$$

We first focus on the diffusive contribution to \dot{M}_2 , which after recalling that $\sum_i \lambda_i \Delta \rho_i^I = 0$ reads

$$\dot{M}_2 \Big|_{\text{diff}} = D \sum_i \lambda_i^2 \Delta \rho_i^I. \quad (\text{S.17})$$

In the continuum limit of Supplementary Note 1, $D \Delta \rho^I \rightarrow \frac{\mathcal{D}}{2} \frac{\partial^2 \rho^I}{\partial \lambda^2}$, where $\mathcal{D} \equiv D(\Delta \lambda)^2$, so that

$$\dot{M}_2 \Big|_{\text{diff}} \simeq \frac{\mathcal{D}}{2} \int \lambda^2 \frac{\partial^2 \rho^I}{\partial \lambda^2} d\lambda. \quad (\text{S.18})$$

Integrating by parts twice and assuming vanishing boundary terms,

$$\int \lambda^2 \frac{\partial^2 \rho^I}{\partial \lambda^2} d\lambda = - \int 2\lambda \frac{\partial \rho^I}{\partial \lambda} d\lambda = 2 \int \rho^I(\lambda, t) d\lambda. \quad (\text{S.19})$$

Since $\int \rho^I d\lambda = B$, we obtain

$$\dot{M}_2 \Big|_{\text{diff}} \simeq \mathcal{D} B. \quad (\text{S.20})$$

Diffusion conserves total prevalence, $\dot{B}|_{\text{diff}} = 0$, so the leading diffusive contribution to the variance evolution is

$$\dot{\text{Var}}(\lambda) \Big|_{\text{diff}} \simeq \mathcal{D}. \quad (\text{S.21})$$

The remaining contribution to $\dot{\text{Var}}(\lambda)$ arises from the selection terms in Eq. (S.8). After expressing $\dot{\text{Var}}(\lambda) = \dot{M}_2/B - (M_2/B^2)\dot{B} - 2\bar{\lambda}\dot{\bar{\lambda}}$, this contribution can be written as a central third-order moment of the trait distribution, i.e. $\dot{\text{Var}}(\lambda) \Big|_{\text{sel}} = k s \langle (\lambda - \bar{\lambda})^3 \rangle_{\rho^I}$. The trait distribution forms a nearly symmetric traveling profile in λ -space, so its skewness is small. Equivalently, at leading order, the distribution is well described by a Gaussian approximation, for which the third central moment vanishes. As a result, this selection-induced contribution is subleading for the sharply peaked initial condition considered here compared to the diffusive term. Therefore, integrating Eq. (S.21) yields

$$\text{Var}(\lambda) \simeq \mathcal{D} t, \quad (\text{S.22})$$

where we used $\text{Var}(\lambda; t=0) \simeq 0$ for a sharply peaked initial condition.

Closed expression for the evolution of the average infectivity

Finally, substituting Eq. (S.22) into Eq. (S.15) yields $\dot{\bar{\lambda}}(t) \simeq k \mathcal{D} s(t) t$, whose integration results in

$$\bar{\lambda}(t) = \lambda_0 + k \mathcal{D} \int_0^t s(t') t' dt', \quad (\text{S.23})$$

as reported in the main text. At early times $s(t') \simeq 1$, giving Eq. (4):

$$\bar{\lambda}(t) \Big|_{t \rightarrow 0} = \lambda_0 + \frac{1}{2} k \mathcal{D} t^2. \quad (\text{S.24})$$

Closed expression for the evolution of the prevalence

Considering the early-time regime $s(t) \simeq 1$ and the evolution of the average infectivity given by Eq. (S.24), we can rewrite Eq. (S.1) as

$$\frac{\partial i(t)}{\partial t} \frac{1}{i(t)} \simeq k \lambda_0 - \mu + \frac{1}{2} k^2 \mathcal{D} t^2 = \mu(R_0 - 1) + \frac{1}{2} k^2 \mathcal{D} t^2, \quad (\text{S.25})$$

where $R_0 \equiv k \lambda_0 / \mu$. Integrating Eq. (S.25) from 0 to t finally yields to Eq. (7):

$$i(t) \Big|_{t \rightarrow 0} = i_0 \exp \left[\mu(R_0 - 1)t + \frac{k^2 \mathcal{D}}{6} t^3 \right], \quad (\text{S.26})$$

which makes explicit the superexponential early-time growth induced by infectivity evolution.

SUPPLEMENTARY NOTE 3: SIGMOID APPROXIMATION OF SUSCEPTIBLE DEPLETION

In this Supplementary Note we expand on Appendix A by providing the detailed derivation of the analytical approximation for the time dependence of the susceptible fraction, and use it to characterize the slowdown of infectivity growth at intermediate times.

In standard SIR dynamics, the susceptible population decreases monotonically from $s(0) \simeq 1$ to its final value $s(\infty) = 1 - r(\infty)$. Although no closed-form expression exists for $s(t)$, its qualitative shape is robust: a slow initial decay, a rapid drop around the epidemic peak, and a final saturation. Motivated by this behavior, we approximate the susceptible fraction by a sigmoid centered at the epidemic peak time t_p ,

$$s(t) \simeq s(\infty) + \frac{1 - s(\infty)}{1 + e^{\sigma(t-t_p)}}. \quad (\text{S.27})$$

The parameters $s(\infty)$, t_p , and σ encode the final epidemic size, the time of maximum prevalence, and the characteristic timescale of susceptible depletion, respectively.

Substituting the sigmoidal approximation (S.27) into Eq.(S.23), which captures the evolution of the average infectivity, yields

$$\bar{\lambda}(t) = \lambda_0 + k\mathcal{D} \left[s(\infty) \frac{t^2}{2} + (1 - s(\infty)) \int_0^t \frac{t'}{1 + e^{\sigma(t'-t_p)}} dt' \right]. \quad (\text{S.28})$$

The remaining integral can be evaluated explicitly. Integrating by parts, one obtains

$$\int_0^t \frac{t'}{1 + e^{\sigma(t'-t_p)}} dt' = -\frac{t-t_p}{\sigma} \frac{e^{-\sigma(t-t_p)}}{1 + e^{-\sigma(t-t_p)}} - \frac{1}{\sigma^2} \frac{e^{-\sigma(t-t_p)}}{1 + e^{-\sigma(t-t_p)}} - \frac{t_p}{\sigma} \frac{e^{-\sigma(t-t_p)}}{1 + e^{-\sigma(t-t_p)}} + \text{const}, \quad (\text{S.29})$$

where the additive constant is fixed so that the integral vanishes at $t = 0$. Substituting Eq. (S.29) into Eq. (S.28) and retaining the dominant contributions for times around and beyond the epidemic peak, we finally obtain Eq. (A1):

$$\bar{\lambda}(t) \sim k\mathcal{D} \left[s(\infty) \frac{t^2}{2} - (1 - s(\infty)) \frac{t-t_p}{\sigma} e^{-\sigma(t-t_p)} \right], \quad (\text{S.30})$$

which makes explicit the presence of a negative transient contribution to the growth of the average infectivity around the epidemic peak, due to susceptible depletion.

SUPPLEMENTARY NOTE 4: HYBRID APPROXIMATION FOR EPIDEMIC CONTROL

In this Supplementary Note we derive the hybrid analytical framework used to characterize epidemic control in the presence of infectivity evolution. The approach considers an intervention applied over a finite time window $[0, \tau]$, during which infectivity evolves under control, followed by a post-intervention phase in which the dynamics proceeds without control and with infectivity fixed to its value at lifting.

Early-time dynamics under intervention

We focus on control strategies applied during a finite intervention window $[0, \tau]$, and distinguish between interventions acting on transmission parameters, either by reducing the contact rate k or the transmission probability λ by a factor $\varepsilon \in (0, 1)$, and interventions acting on the recovery rate μ . As shown in Supplementary Note 2, the evolution of the average infectivity follows from differentiating $\bar{\lambda} = \sum_i \lambda_i \rho_i^I / \sum_i \rho_i^I$ and substituting the dynamical equation for $\dot{\rho}_i^I$ (Eq. (S.8), which is the discrete version of Eq. (1)). Importantly, only the transmission term $\lambda_i k \rho_i^I s$ contributes to the selective amplification of higher-infectivity strains, whereas the recovery term cancels out in the derivation of $\dot{\bar{\lambda}}(t)$, yielding $\dot{\bar{\lambda}}(t) = k s(t) \text{Var}(\lambda)$ (see Supplementary Note 2), which depends explicitly on the transmission process but not on the recovery rate.

As a consequence, control interventions modify infectivity evolution only if they rescale the transmission term in Eq. (S.8). For k - or λ -control, the transmission term is multiplied by ε , so the same factor appears in the selection term driving $\dot{\bar{\lambda}}$. In contrast, μ -control alters only the recovery term, which does not contribute to $\dot{\bar{\lambda}}(t)$, and therefore does not affect the selective amplification mechanism. Accordingly, the effect of control on infectivity evolution can be encoded in a single parameter α , capturing whether the intervention rescales the selection term. During the intervention, the evolution of the average infectivity can be written in the unified form

$$\dot{\bar{\lambda}}(t) = \alpha k s(t) \text{Var}(\lambda), \quad (\text{S.31})$$

where $\alpha = \varepsilon$ for interventions acting on transmission (k - or λ -control), and $\alpha = 1$ for interventions acting on the recovery rate μ .

Assuming that the intervention occurs during early-time dynamics, prevalence remains small and we approximate $s(t) \simeq 1$. Using the early-time growth of the variance derived in Eq. (S.22) of Supplementary Note 2, $\text{Var}(\lambda) \simeq \mathcal{D} t$, integration of Eq. (S.31) yields to Eq. (8):

$$\bar{\lambda}(t, \varepsilon) = \lambda_0 + \frac{1}{2} \alpha k \mathcal{D} t^2. \quad (\text{S.32})$$

The evolution of the epidemic prevalence during an early-time intervention follows from the equation

$$\frac{di(t)}{dt} \frac{1}{i(t)} = \beta_c(t) - \mu_c, \quad (\text{S.33})$$

where $\beta_c(t)$ and μ_c denote the effective transmission and recovery rates under control.

For interventions acting on transmission (k - or λ -control), the force of infection is rescaled by a factor ε , yielding $\beta_c(t) = \varepsilon k \bar{\lambda}(t)$ and $\mu_c = \mu$. In contrast, for interventions acting on the recovery rate (μ -control), the transmission process is unaltered, so that $\beta_c(t) = k \bar{\lambda}(t)$, whereas the recovery rate is rescaled as $\mu_c = \mu/\varepsilon$. Substituting Eq. (S.32) into Eq. (S.33) and integrating from 0 to t gives

$$i(t, \varepsilon)|_{t \rightarrow 0} = i_0 \exp \left[\frac{\mu \alpha}{\varepsilon} (\varepsilon R_0 - 1) t + \frac{\alpha^2 k^2}{6} \mathcal{D} t^3 \right]. \quad (\text{S.34})$$

which coincides with Eq. (9). Eq. (S.34) shows explicitly the coexistence of a linear epidemiological contribution, controlled by the intervention, and a positive evolutionary contribution scaling as t^3 .

Variation of the post-intervention peak

We now derive an explicit expression for the variation of the post-intervention epidemic peak with respect to the lifting time τ within the hybrid approximation introduced above. We assume that the global peak occurs after lifting

the intervention, i.e., the maximum prevalence is attained for $t > \tau$, and denote by $(s(\tau), i(\tau), r(\tau))$ the state at the lifting time. After $t = \tau$, we approximate the system dynamics to follow an uncontrolled SIR process with recovery rate μ and transmission rate $\beta(\tau)$ set by the infectivity at lifting, $\beta(\tau) = k\bar{\lambda}(\tau)$. The basic reproduction number immediately after lifting is therefore $\mathcal{R}_0(\tau) = \beta(\tau)/\mu = k\bar{\lambda}(\tau)/\mu$.

For an SIR outbreak with constant basic reproduction number R_0 starting from (s_0, i_0, r_0) , the infected fraction reaches its maximum when $s = 1/R_0$. Using the SIR invariant

$$r(t) + \frac{1}{R_0} \ln s(t) = r_0 + \frac{1}{R_0} \ln s_0, \quad (\text{S.35})$$

and imposing the condition $s_{\text{peak}} = 1/R_0$, one obtains the peak prevalence

$$i_{\text{max}} = 1 - r_0 - \frac{1}{R_0} [1 + \ln(R_0 s_0)]. \quad (\text{S.36})$$

Applying Eq. (S.36) to the post-lifting outbreak with $(s_0, i_0, r_0) = (s(\tau), i(\tau), r(\tau))$ and $R_0 = \mathcal{R}_0(\tau)$ yields Eq. (A2):

$$i_{\text{max}}(\tau) = 1 - r(\tau) - \frac{1}{\mathcal{R}_0(\tau)} [1 + \ln(\mathcal{R}_0(\tau)s(\tau))], \quad (\text{S.37})$$

where $s(\tau) = 1 - i(\tau) - r(\tau)$.

We now differentiate Eq. (S.37) with respect to τ using the chain rule, which yields

$$\frac{di_{\text{max}}}{d\tau} = -\dot{r}(\tau) + \frac{\dot{\mathcal{R}}_0(\tau)}{\mathcal{R}_0(\tau)^2} [1 + \ln(\mathcal{R}_0(\tau)s(\tau))] - \frac{1}{\mathcal{R}_0(\tau)} \left(\frac{\dot{\mathcal{R}}_0(\tau)}{\mathcal{R}_0(\tau)} + \frac{\dot{s}(\tau)}{s(\tau)} \right) \quad (\text{S.38})$$

$$= -\dot{r}(\tau) + \frac{\dot{\mathcal{R}}_0(\tau)}{\mathcal{R}_0(\tau)^2} \ln(\mathcal{R}_0(\tau)s(\tau)) - \frac{1}{\mathcal{R}_0(\tau)} \frac{\dot{s}(\tau)}{s(\tau)}. \quad (\text{S.39})$$

During the controlled phase $t \in [0, \tau]$, the SIR equations imply

$$\dot{r}(\tau) = \mu_c i(\tau), \quad \dot{s}(\tau) = -\beta_c(\tau) s(\tau) i(\tau), \quad (\text{S.40})$$

where $\beta_c(\tau)$ and μ_c denote the controlled transmission and recovery rates, respectively. Recall that the post-lifting outbreak is approximated as an uncontrolled SIR process with transmission rate $\beta(\tau) = k\bar{\lambda}(\tau)$ and baseline recovery rate μ . Using $\dot{s}(\tau)/s(\tau) = -\beta_c(\tau) i(\tau)$, Eq. (S.39) can be rewritten as

$$\frac{di_{\text{max}}}{d\tau} = -\mu_c i(\tau) + \frac{\dot{\mathcal{R}}_0(\tau)}{\mathcal{R}_0(\tau)^2} \ln(\mathcal{R}_0(\tau)s(\tau)) + \frac{\beta_c(\tau)}{\mathcal{R}_0(\tau)} i(\tau). \quad (\text{S.41})$$

Introducing α such that $\alpha = \varepsilon$ for interventions acting on transmission (k - or λ -control), whereas $\alpha = 1$ for interventions acting on the recovery rate (μ -control), Eq. (S.41) can be written in the compact form

$$\frac{di_{\text{max}}}{d\tau} = -\mu i(\tau) \alpha \frac{(1 - \varepsilon)}{\varepsilon} + \frac{\dot{\mathcal{R}}_0(\tau)}{\mathcal{R}_0(\tau)^2} \ln(\mathcal{R}_0(\tau)s(\tau)). \quad (\text{S.42})$$

Finally, using the early-time evolution of the average infectivity during the intervention, $\bar{\lambda}(\tau) = \lambda_0 + \alpha k D \tau^2 / 2$, we obtain

$$\dot{\mathcal{R}}_0(\tau) = \frac{\alpha k^2}{\mu} D \tau, \quad (\text{S.43})$$

which, substituted into Eq. (S.42), yields the unified expression reported in Eq. (10) of the main text.

Critical diffusion strength

The onset of nonmonotonic epidemic responses is determined by the existence of intervention durations τ for which the post-lifting epidemic peak satisfies $di_{\text{max}}/d\tau = 0$. Using Eq. (8) of the main text and evaluating all quantities at lifting, this condition can be written explicitly as

$$\mu \alpha \frac{(1 - \varepsilon)}{\varepsilon} i(\tau) = \frac{\alpha k^2}{\mu} D \tau \frac{\ln(\mathcal{R}_0(\tau)s(\tau))}{\mathcal{R}_0(\tau)^2}, \quad (\text{S.44})$$

where $\alpha = \varepsilon$ for transmission-based control (k - or λ -control) and $\alpha = 1$ for recovery-based control (μ -control). Equation (S.44) expresses a balance between a negative epidemiological contribution proportional to the prevalence accumulated during the intervention (left-hand side) and a positive evolutionary contribution driven by the increase of the time-varying basic reproduction number due to infectivity evolution (right-hand side). Since $\alpha > 0$, it cancels from both sides, yielding the implicit relation reported in Eq. (A3):

$$\mathcal{D}_c(\tau) = \frac{\mu^2(1-\varepsilon) i(\tau) \mathcal{R}_0(\tau)^2}{\varepsilon k^2 \tau \ln(\mathcal{R}_0(\tau)s(\tau))}. \quad (\text{S.45})$$

To obtain an explicit expression, we assume that the prevalence remains small at lifting and that the dominant contribution encoding evolutionary effects enters through the prevalence $i(\tau)$. Accordingly, we approximate $s(\tau) \simeq 1$, $\ln(\mathcal{R}_0(\tau)s(\tau)) \simeq \ln R_0$ and $\mathcal{R}_0(\tau) \simeq R_0$. Under these approximations, Eq. (S.45) reduces to

$$\mathcal{D}_c(\tau) \simeq \frac{\mu^2(1-\varepsilon) R_0^2}{\varepsilon k^2 \tau \ln R_0} i(\tau). \quad (\text{S.46})$$

We now substitute the early-time prevalence at lifting in its unified form,

$$i(\tau) \simeq i_0 \exp\left[\frac{\mu\alpha}{\varepsilon} (\varepsilon R_0 - 1) \tau + \frac{\alpha^2 k^2}{6} \mathcal{D}_c(\tau) \tau^3\right], \quad (\text{S.47})$$

where $\alpha = \varepsilon$ for k - or λ -control and $\alpha = 1$ for μ -control. Substituting Eq. (S.47) into Eq. (S.46) yields

$$\mathcal{D}_c(\tau) \simeq \frac{\mu^2(1-\varepsilon) R_0^2}{\varepsilon k^2 \tau \ln R_0} i_0 \exp\left[\frac{\mu\alpha}{\varepsilon} (\varepsilon R_0 - 1) \tau + \frac{\alpha^2 k^2}{6} \mathcal{D}_c(\tau) \tau^3\right]. \quad (\text{S.48})$$

Defining

$$P(\tau) = \frac{1}{6} \alpha^2 k^2 \tau^3, \quad Q(\tau) = \frac{\mu^2(1-\varepsilon) R_0^2}{\varepsilon k^2 \tau \ln R_0} i_0 \exp\left[\frac{\mu\alpha}{\varepsilon} (\varepsilon R_0 - 1) \tau\right], \quad (\text{S.49})$$

Eq. (S.48) can be written as $-P(\tau)\mathcal{D}_c(\tau) e^{-P(\tau)\mathcal{D}_c(\tau)} = -P(\tau)Q(\tau)$, so that the solution can be expressed in closed form as in Eq. (A4) using the Lambert W function, defined by $W(x)e^{W(x)} = x$:

$$\mathcal{D}_c(\tau) = -\frac{1}{P(\tau)} W_0[-P(\tau)Q(\tau)]. \quad (\text{S.50})$$

Here W_0 denotes the relevant real branch of the Lambert function. Due to the assumptions of our hybrid approximation, this expression diverges $\mathcal{D}_c(\tau) \rightarrow \infty$ as $\tau \rightarrow 0$, while capturing the existence of a finite critical effective diffusion strength for small but finite intervention durations.

Critical intervention duration

When evolutionary effects are present, the post-lifting epidemic peak $i_{\max}(\tau)$ is no longer monotonic in the intervention duration τ . An interior extremum $\tau^* > 0$ is determined by the condition $di_{\max}/d\tau = 0$. Using Eq. (8) of the main text and evaluating all quantities at the lifting time, the condition $di_{\max}/d\tau = 0$ can be written as

$$\mu \frac{(1-\varepsilon)}{\varepsilon} i(\tau) = \frac{k^2}{\mu} \mathcal{D} \tau \frac{\ln(\mathcal{R}_0(\tau)s(\tau))}{\mathcal{R}_0(\tau)^2}, \quad (\text{S.51})$$

Assuming early-time dynamics and that the dominant evolutionary contribution enters through the prevalence at lifting, we approximate $s(\tau) \simeq 1$, $\mathcal{R}_0(\tau) \simeq R_0$, and $\ln(\mathcal{R}_0(\tau)s(\tau)) \simeq \ln R_0$. Under these conditions, Eq. (S.51) reduces to

$$\mu \frac{(1-\varepsilon)}{\varepsilon} i(\tau) \simeq \frac{k^2}{\mu} \mathcal{D} \tau \frac{\ln R_0}{R_0^2}. \quad (\text{S.52})$$

Substituting Eq. (7) into Eq. (S.52) yields the transcendental equation

$$C \mathcal{D} \tau = \mu \frac{(1-\varepsilon)}{\varepsilon} i_0 \exp[A\tau + B \mathcal{D} \tau^3], \quad (\text{S.53})$$

with

$$A = \frac{\mu\alpha}{\varepsilon} (\varepsilon R_0 - 1), \quad B = \frac{\alpha^2 k^2}{6}, \quad C = \frac{k^2 \ln R_0}{\mu R_0^2}, \quad (\text{S.54})$$

and α encoding the effect of the control strategy, being $\alpha = \varepsilon$ for interventions acting on transmission (k - or λ -control), whereas $\alpha = 1$ for interventions acting on the recovery rate (μ -control). In the regime where the cubic evolutionary term dominates the exponent, $BD\tau^3 \gg |A\tau|$, Eq. (S.53) simplifies to

$$C\mathcal{D}\tau \simeq \mu \frac{(1-\varepsilon)}{\varepsilon} i_0 \exp(B\mathcal{D}\tau^3). \quad (\text{S.55})$$

Defining $x \equiv 3BD\tau^3$, one obtains

$$x e^x = -\frac{3B\mu^3(1-\varepsilon)^3 i_0^3}{\varepsilon^3 C^3 \mathcal{D}^2}, \quad (\text{S.56})$$

and finally, using the definition of the Lambert function, $W(z)e^{W(z)} = z$, we reach Eq. (11) in the main text:

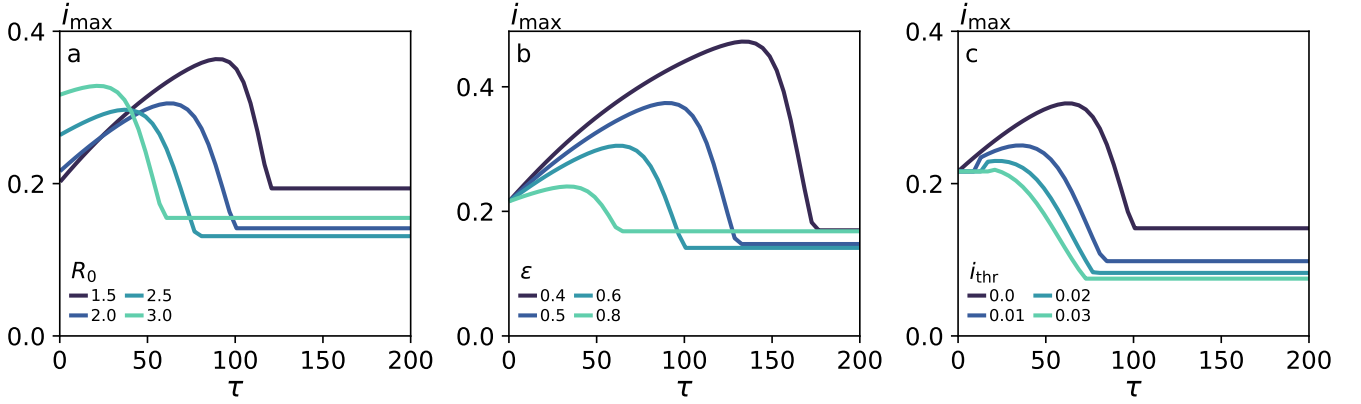
$$\tau^* \simeq \left[-\frac{1}{3BD} W_{-1} \left(-\frac{3B\mu^3(1-\varepsilon)^3 i_0^3}{\varepsilon^3 C^3 \mathcal{D}^2} \right) \right]^{1/3}. \quad (\text{S.57})$$

The argument of the Lambert function is negative, so two real branches may exist whenever $-1/e < z < 0$. The physically relevant solution corresponding to an interior maximum of $i_{\max}(\tau)$ is obtained from the W_{-1} branch. The principal branch W_0 yields a small- τ solution that corrects an initial decreasing trend introduced by the hybrid approximation.

SUPPLEMENTARY NOTE 5: ROBUSTNESS OF THE NONMONOTONIC EPIDEMIC RESPONSE

In Fig. 2 of the main text, we showed that infectivity evolution induces a nonmonotonic dependence of the post-intervention epidemic peak i_{\max} on the intervention duration τ . In Supplementary Fig. 1 we assess the robustness of this behavior under variations of key epidemiological parameters, while keeping the effective diffusion strength fixed at $\mathcal{D} = 10^{-6}$. We independently vary: the initial basic reproduction number R_0 in Fig. 1.a, the intervention strength ε in Fig. 1.b, and the activation threshold i_{thr} in Fig. 1.c, which determines the prevalence level at which the intervention is triggered. Specifically, the control policy is implemented once the infected fraction satisfies $i(t) = i_{\text{thr}}$. Thus, $i_{\text{thr}} = i_0$ corresponds to an intervention applied immediately at the onset of the outbreak, whereas larger values of i_{thr} delay the implementation of control, allowing the epidemic and infectivity evolution to progress before intervention.

In all cases, the qualitative nonmonotonic behavior persists. Increasing τ increases the post-lifting epidemic peak until a critical value τ^* . After that, the peak decreases with τ . Quantitatively, increasing R_0 shifts the maximum toward smaller intervention durations. Varying the intervention strength ε modulates the balance between epidemiological suppression and evolutionary amplification: stronger interventions (smaller ε) advance the onset of the maximum and reduce its amplitude. Finally, changes in i_{thr} effectively rescale the initial conditions of the epidemic trajectories. This affects the early-time accumulation of evolutionary effects and therefore alter the location of the maximum. Overall, these results confirm that the nonmonotonous behavior is robust across a broad region of parameter space.



Supplementary Fig. 1. **Robustness of the nonmonotonic epidemic impact.** Epidemic peak i_{\max} as a function of the intervention duration τ . Columns show the dependence on: **a** the initial basic reproduction number R_0 , **b** the intervention strength ε , and **c** the activation threshold i_{thr} . Unless otherwise varied, parameters are $R_0 = 2$, $\varepsilon = 0.6$, $i_{\text{thr}} = 0$, $i_0 = 10^{-3}$, $\mu = 1/7$, $k = 10$, $\mathcal{D} = 10^{-6}$ and $\Delta\lambda = 10^{-3}$.